Electro-magnetic Tooling for Metal Forming and Powder Compaction: Numerical Simulation

A.G. Mamalis[1], D.E. Manolakos[1], A.G. Kladas[2], A.K. Koumoutsos[1]

[1] Manufacturing Technology Division National Technical University of Athens, Greece
[2] Electric Power Division National Technical University of Athens, Greece

Abstract

The multipurpose FE Code ANSYS is employed to simulate an electro-magnetic forming process. A complicated compression coil with a ferromagnetic outer screen and a stepped field shaper is considered. Details on FE model building are thoroughly discussed. The calculated parameters are the magnetic flux density around the conductors as well as the Lorentz forces developed in both the field shaper and the workpiece. A simplified analysis of the workpiece deformation characteristics is also provided. An equivalent circuit method is employed in order to validate the results from the electro-magnetic FE model. Results from both analyses are in good agreement, denoting that the FE results are valid from an engineering point of view.

Keywords:

Electro-magnetic forming, Tool analysis, Tube compression

1 Introduction

In industrial practice, the tools of electro-magnetic forming and dynamic compaction processes are more complicated than a single-layer solenoid winding [1,2]. For this reason, the analytical calculation of the magnetic pressure acting on the workpiece is very difficult. However, electro-magnetic forming has been widely applied in aerospace and automotive industry since its economic restriction to relatively small parts has allowed trial - and - error development to overcome the handicap of the existing lack of knowledge. In literature, there are only a few papers on the analytical calculation of the magnetic field when a field shaper is employed in an electro-magnetic forming process [3-6]. The most effective approach, from an engineering point of view, is the equivalent circuit method proposed by Göbl [7]. Furthermore, useful engineering calculations regarding the thermal as well as the mechanical aspects of field shapers design are found in references [8,9]. In the present paper, a finite element analysis of an industrial compression coil contributes to the more systematic analysis of the process, offering valuable information for tooling design.

2 Model Description

2.1 The Electro-Magnetic Model

The Multiphysics High Option, Release 6 version of ANSYS is employed for the modelling of the forming coil. The drawing of the forming coil is presented in Figure 1a/b. It is a single-layer, four-turn solenoid coil with a ferromagnetic outer screen and a stepped field shaper. Due to the slit existence, the problem cannot be treated as axisymmetric. So, a 3D modelling is applied and since the tool possesses both a transverse and a longitudinal plane of symmetry, the simulation may be conducted considering the geometry shown in Figure 1c.

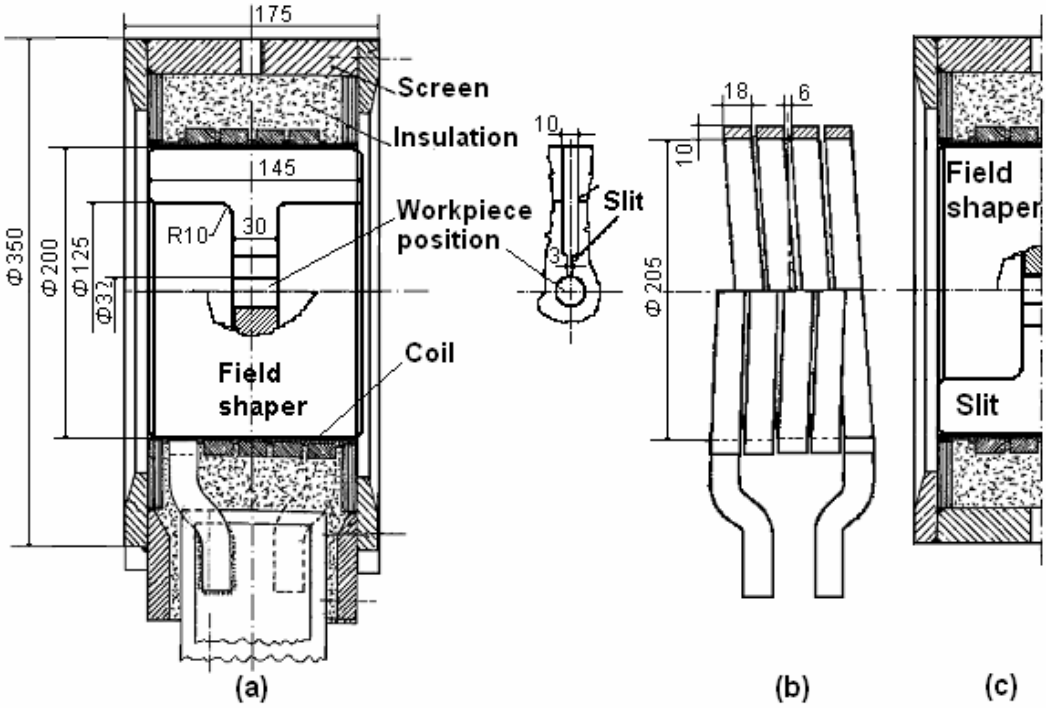

Figure 1: *The electro-magnetic forming tool for tube compression and powder compaction (a) the tool assembly, (b) the coil winding, and (c) the simulated region of the tool*

The above-mentioned code has a limitation of 32000 elements or nodes. A mapped-meshing type is selected, enabling the exact determination of the number of nodes and elements. So, the model applied is practically a plain lattice swept around its axis in order to create the corresponding volume, see Figure 2. The first block (0°- 171°) is the main block, the second block (171°- 175°) represents the region near the slit, and the third block (175°- 180°) corresponds to the slit region. The slit direction is assumed radial rather than transverse for modelling simplification. In electro-magnetic forming practice the width of the slit just above the workpiece is crucial, because the magnetic pressure is reduced in this area. In the drawing of the forming tool this gap is given 3 mm, while in the model this gap is actually a small arc, which length is given by the product of the angle of the third block times the radius of the hole of the field shaper, i.e. $[(5/180)\cdot\pi]\cdot 16 = 1.4 \approx 3/2 = 1.5$ mm, which is acceptable.

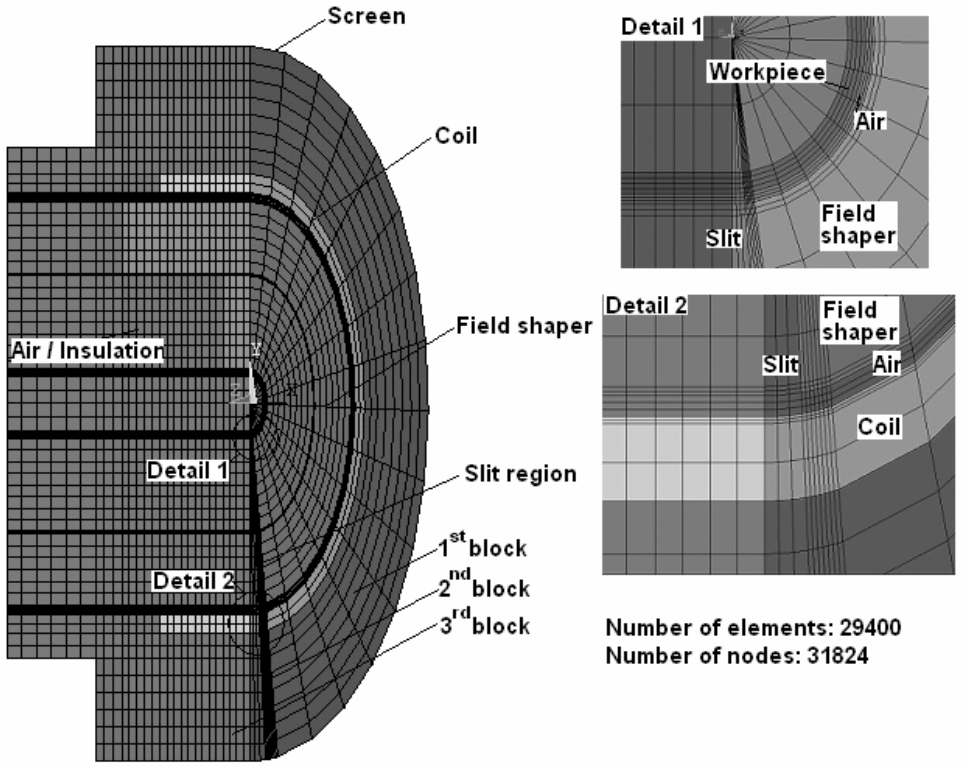

Figure 2: *The meshing of the electro-magnetic model*

The necessary material properties of each entity of the model and the chosen element type with their corresponding degrees of freedom are given in Table 1. The nodal and the element coordinate system are rotated to the local cylindrical coordinate system WX, WY, WZ, according to the orientation indicated in Table 2. The boundary conditions and loads are also referred to the local cylindrical coordinate system. However, in all figures the depicted coordinate system of the model as well as of the results is the global Cartesian one. The main load is the current flowing in the coil. In practice, it can be easily measured by means of a Rogowski coil connected to an oscilloscope. In the electro-magnetic forming process the current is approximately expressed by the following equation:

$$I(t) = I_o \cdot exp(-\gamma \cdot t) \cdot sin(\omega_d \cdot t) \tag{1}$$

where, I_0 = 124600A, γ = 4805.8 s^{-1}, ω_d = 43564 rad/s in the present analysis. This current is produced by a discharge of 6 kV stored in a capacitor bank of 480 μF. Due to the transient nature of the process, the current flows near the surface of the conductors. The penetration depth of each conductor can be calculated via the well-known equation

$$\delta = \sqrt{\frac{2 \cdot \rho_e}{\mu_r \cdot \mu_o \cdot \omega_d}} \tag{2}$$

where, μ_0 = 4 π 10^{-7} H/m. Finite element analysis requires at least one or two elements through the penetration depth.

S/N	Entity - Material	ρ_e $10^{-8}\cdot$ [Ω·m]	μ_r	Element	Degrees of freedom
1	Coil - Cu	1.79	1	SOLID97	A_x, A_y, A_z[(a)], Volt[(b)]
2	Workpiece - Al	3.33	1	SOLID97	A_x, A_y, A_z, Volt
3	Screen - Mild Steel		100	SOLID96	Mag[(c)]
4	Field shaper - Al	3.33	1	SOLID97	A_x, A_y, A_z, Volt
5	Surroundings - Air or Insulator		1	SOLID97	A_x, A_y, A_z
6	Interface (3) / (5)			INTER115	

[(a)] A: The magnetic vector potential and X, Y, Z, the radial, tangential and axial component, respectively
[(b)] Volt: The time-integrated potential
[(c)] Mag: The magnetic scalar potential

Table 1: *The data of the electro-magnetic model*

According to the above mentioned details and taking into account that the radius of the inner hole of the field shaper is 16 mm and that the angle of the block, which represents the region near the slit, is 4°, then it should be checked that the inner arc of the field shaper part, which belongs to this block, is bigger than its skin depth. Indeed, (4°/180°) π 16 = 1.12 mm > δ_{Al} = 1.11 mm, which is valid. Furthermore, the necessary number of elements in the tangential direction can be found if the outer arc of the same block of the field shaper is divided by the skin depth, i.e. (4°/180°)·π·100/1.11 = 6.28, so seven elements are enough. The mesh density in the rest of the model is selected according to the general rule that the mesh density should be proportional to the energy density, e.g. the energy density is high in the gaps between two adjacent current carrying conductors, see Figure 2. Load and boundary conditions are both applied to nodes. In the transverse and longitudinal plane of symmetry, flux normal and flux parallel boundary conditions are established respectively. An additional entity with air elements has been placed adjacent to the free bound of the modelled part of the tool in order to enhance the development of the magnetic field, since it is very difficult to establish the required far field boundary conditions there, see Figure 2. A more detailed presentation of the boundary conditions is given in Table 3.

Components of a common cylindrical coordinate system	Local cylindrical coordinate system	Global Cartesian coordinate system
Radial	WX	+Y
Tangential	WY	-Z
Axial	WZ	-X

Table 2: *Determination of the coordinate system used in the model*

The coil is considered to be a single-turn for modelling simplification, so the input current (I_{eq}) should be corrected with a factor in order to ensure that the induced magnetic field is approximately the same in both cases, according to the approximate relation:

$$\frac{N \cdot I(t)}{\ell_1} = \frac{1 \cdot I_{eq}(t)}{0.5 \cdot \ell_1} \Rightarrow I_{eq}(t) = 0.5 \cdot N \cdot I(t) \tag{3}$$

where, N = 4, the number of the coil turns and ℓ_1: the coil length. Equation (3) is valid for long coils. However, it is employed for the present coil, which is short (i.e. the diameter is comparable to the length), because the flux is entrapped in small gaps and its pattern consists of parallel straight lines.

S/N	WZ=0	WY=0	WY=180o	WX=150 [mm]	WX=125 [mm]	WZ=72.5 [mm]
1	A_z=0	Volt=0 (in skin depth), A_x=A_z=0	Couple volt in skin depth, A_x=A_z=0			
2	A_z=0	Volt=0, A_x=A_z=0	Volt=0, A_x=A_z=0			
3	Mag=0					
4	A_z=0	Volt=0 (in skin depth), A_x=A_z=0				
5	A_z=0	A_x=A_z=0	A_x=A_z=0			
6				A_x=0	A_x=0	A_z=0

Table 3: *The entities and their areas onto which boundary conditions are applied*

The current is applied in transient analysis in increments of 1 microsecond. Only the first half of the current period is considered, because it corresponds to the first peak of magnetic pressure, which is assumed to be responsible for the plastic work produced on the workpiece. Another assumption that has been considered is that the current is applied in the inner skin depth of the coil. In fact, the current flows all around the surface of the coil winding. But in the present model the inductive coupling between the outer surface of the coil and the screen is ignored, because the selected type of analysis (Magnetic Vector Potential - Nodal Based) cannot treat eddy currents in ferromagnetic materials. So, the outer screen serves only as a “ferromagnetic trap” for the flux outside the coil. The workpiece deformation and its influence on the magnetic field evolution and the resulting forces are disregarded from the present analysis. Moreover, some further assumptions and restrictions possessed by the present model are the following:

- The workpiece thickness (2 mm) is bigger than its skin depth (1.11 mm) and the length of both workpiece and field shaper is equal. These restrictions are possessed by the equivalent circuit method.
- The workpiece material is non-magnetic.
- The current frequency is lower than 30 kHz, thus no electro-magnetic wave effects are considered.
- All the contributing materials are isotropic.
- The temperature dependence of material properties is ignored.

2.2 The Structural Model

The loosely coupling approach is considered; i.e. calculating first the Lorentz forces, neglecting the influence of workpiece deformation on magnetic field evolution, and applying them as input load to the mechanical problem. In the electro-magnetic compression proc-

ess only moderate deformations are usually desirable due to the limitation imposed by the wrinkling defect. So, the abovementioned simplification may be acceptable in many cases; however, experimental validation is always required.

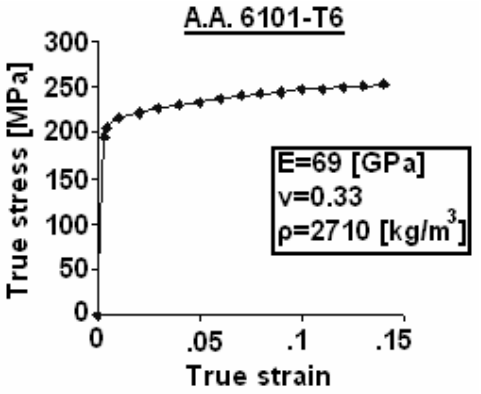

Figure 3: *The mechanical properties of the workpiece*

The structural model consists only of the workpiece. The applied load is the mean magnetic pressure acting on the part of the workpiece, which lies in the middle step of the field shaper (i.e. the sum of the radial component of Lorentz forces divided by the corresponding external area of the workpiece, see below). The tangential distribution of the magnetic pressure cannot be taken into account, because during the simulation the forces are unbalanced in radial direction and the solid-body motion is inevitable. The axial distribution of the magnetic pressure can be neglected. Regarding the abovementioned considerations the model can be 2D axisymmetric, which means more simplicity and less CPU time. The properties of the workpiece material are presented in Figure 3. The model is meshed in a mapped pattern via the four-node PLANE182 element, which is suitable for large deformations of elastoplastic materials. In the present model X, Y, Z axes represent the radial, axial, and tangential directions respectively. Finally, the axial displacement of the nodes, which lie in the transverse plane of symmetry, should be constrained.

3 Results and Discussion

By deriving Equation (1) it yields that the maximum of the input current occurs at 33.5 μs. According to Figure 4(a), the time variation of magnetic flux density follows the one of the input current, as it is expected.

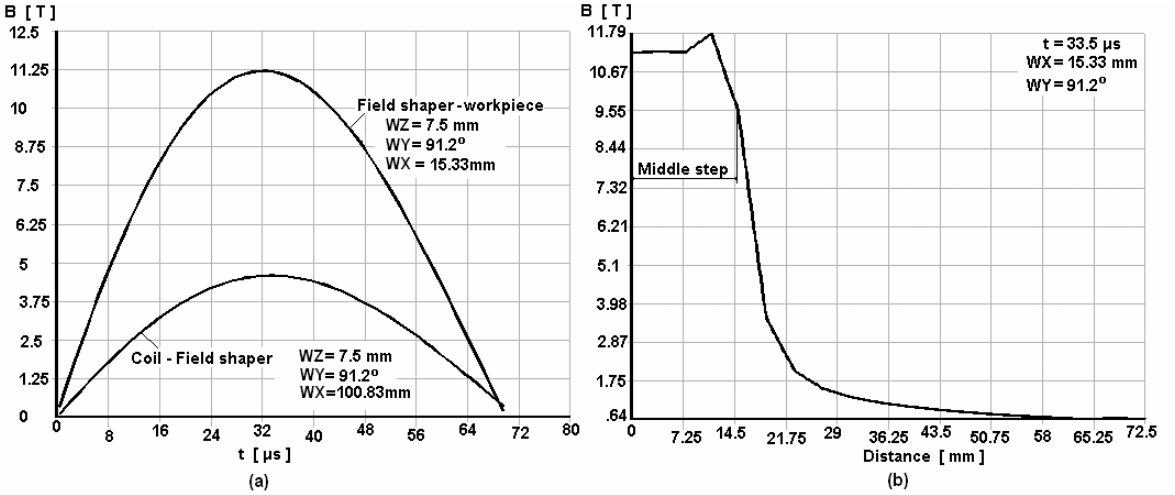

Figure 4: *(a) The magnetic flux density in the gap between the coil and the field shaper as well as between the field shaper and the workpiece vs. time. (b) The distribution of the maximum magnetic flux density along the gap between the field shaper and the workpiece*

The maximum magnetic flux density in the gap between the coil and the field shaper occurs at 33.5 μs, while in the gap between the field shaper and the workpiece the maximum occurs at 31.5 μs, but this difference is negligible. From Figure 4(b) it yields that only at the centre of the middle step of the field shaper the magnetic flux density is uniformly distributed in the axial direction. Outside the middle step the magnetic flux density is sharply reduced, as it is expected [4,5]. However, the distribution of magnetic flux density around the periphery of the gap between the field shaper and the workpiece is not uniform, as it can be seen from Figure 5a. With increasing distance to the slit, the magnetic flux density increases with a decrescent rate. A similar graph can also be obtained for the gap between the coil and the field shaper, see Figure 5b.

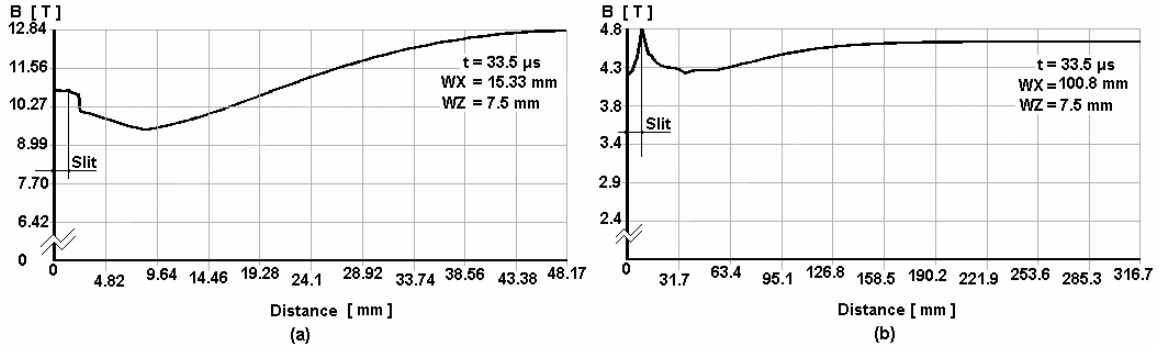

Figure 5: *The distribution of magnetic flux density around the periphery in the gap (a) between the field shaper and the workpiece, and (b) between the coil and the field shape*

The mean magnetic flux density can be calculated according to the following integrals:

$$B_{C-FS} = \frac{1}{307.8} \cdot \int_{8.8}^{316.6} B_{C-FS} \cdot ds \Rightarrow B_{C-FS} = 4.54T \tag{4}$$

and

$$B_{FS-W} = \frac{1}{46.8} \cdot \int_{1.34}^{48.14} B_{FS-W} \cdot ds \Rightarrow B_{FS-W} = 11.25T \tag{5}$$

for the gap between the coil and the field shaper and between the field shaper and the workpiece respectively, excluding the slit region. The corresponding results according to the equivalent circuit method (see Appendix) are $B_{C\text{-}FS}$ = 4.6 T and $B_{FS\text{-}W}$ = 11.3 T, respectively. The results from the two methods are in good agreement, so the FE model is valid from an engineering point of view. It is notable that the latter method meets some limitations (e.g. the case of a very short workpiece), in contrast to the FE analysis, whose capabilities are practically unlimited. Another way to validate the results is the experimental measurement by means of search coils placed in the relevant gaps and connected to a memory oscilloscope.

In fact, the real forces acting on the workpiece will be lower than those presented in Figure 6, because the gap between the field shaper and the workpiece will increase due to the latter's deformation. From Figure 6 it can also be seen that the Lorentz forces on the part of the workpiece under the slit region decrease, as it has been already discussed. The Lorentz force action on the field shaper tends to split it in the slit region (Figure 6). For this reason, a rubber bandage is often placed around the field shaper above the middle step region. This bandage fits tightly the field shaper to the inner insulation of the coil thus preventing the failure of the former.

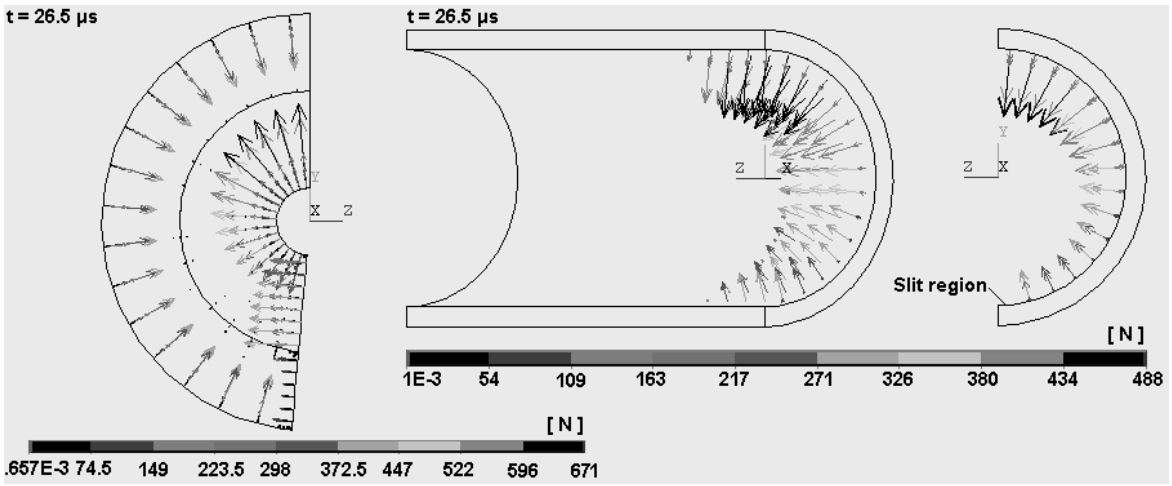

Figure 6: *A vectorial depiction of the Lorentz force distribution over the field shaper and the workpiece*

The final shape of the workpiece is shown in Figure 7a. The central part of the workpiece gains the maximum deformation velocity, which reaches the value of 53.5 m/s at 43 µs, resulting in an equivalent plastic strain rate of 3967 s^{-1}. The deformation process is practically fulfilled at 60 µs, see Figure 7b. The accuracy of the presented results should be

confirmed experimentally. However, they give a first sense regarding the order of magnitude of the corresponding parameters.

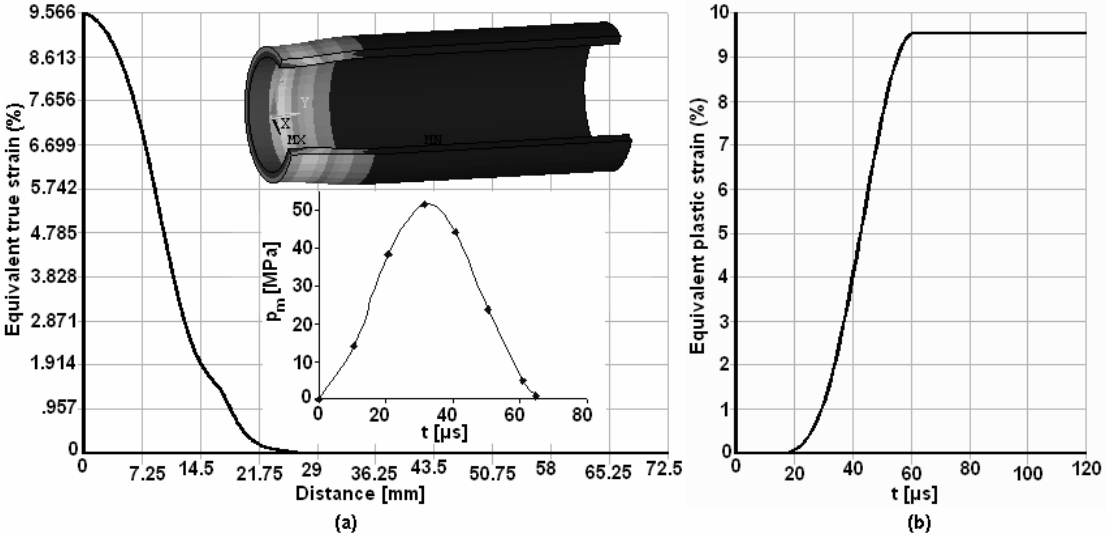

Figure 7: *(a) The final shape of the workpiece and the distribution of the equivalent plastic strain along the workpiece as well as the variation of the mean magnetic pressure vs. time. (b) The equivalent plastic strain in the middle of the workpiece vs time*

4 Conclusions

In the present paper, a methodology based on FE for calculating the operational parameters of the electro-magnetic forming process is presented. An industrial compression coil of complicated geometry is considered. The results of magnetic flux density are valid from an engineering point of view, since they are in close accordance with those obtained from the equivalent circuit method. A simplified analysis of the deformation characteristics of the workpiece is also attained. All the obtained results are consistent to the theory. However, the tenability of the various assumptions considered during the simulation process should be experimentally confirmed. The present analysis can be further developed if the coupling nature of each aspect of the process is taken into account.

References

[1] *Lange, K.:* Handbook of metal forming, McGraw-Hill, 1985, p.27.32-27.39.

[2] *Livshitz, Y.; Gafri, O.:* Technology and equipment for industrial use of pulse magnetic fields, IEEE International Pulsed Power Conference, vol.1, 1999, p.475-478.

[3] *Wilson, M.N.; Srivastava, K.D.:* Design of efficient flux concentrators for pulsed high magnetic fields, Rev. of Sci. Instr. 36 (8), 1965, p.1096-1100.

[4] *von Dietz, H; Lippmann, H.-J.; Schenk, H.:* Theorie des Magneform – Verfahrens: Erreichbarer Druck, ETZ-A ,88 (9), 1967, p. 217-222.

[5] *von Dietz, H; Lippmann, H.-J.; Schenk, H.:* Theorie des Magneform – Verfahrens: Abgestufter Feldkonzetrator, ETZ-A, 88(19), 1967, p.475-780.

[6] *Serbanescu, M.:* Calculation of the magnetic field intensity for slotted field concentrators, Rev. Roum. Sci. Tech.-Electrotechn. Et Energ., 21 (3), 1976, p.365-376.

[7] *Göbl, N.:* Unified calculating method of equivalent circuits of electro-magnetic forming tools, PhD Thesis, Tech. Univ. of Budapest, Fac. of Elec. Eng., 1978.

[8] *Batygin, Y.V.; Daehn, G.S.:* The pulse magnetic fields for progressive technologies, Monograph, Kharkov-Columbus, 1999, available at: http://www.er6.eng.ohio-state.edu/~DAEHN/hyperplasticity.html.

[9] *Altynova, M.M.:* Electro-magnetic metal forming handbook, Mat. Sci. and Eng. Dept, The Ohio State Univ., Transl. of the Russian book: SPRAVOCHNIK PO MAGNITNO-IMPUL' SNOY OBRABOTKE METALLOV by IV Belyy, SM Fertik and LT Khimenko, VISCHA SHKOLA available at: http://www.er6.eng.ohio-state.edu/~DAEHN/hyperplasticity.html.

Appendix

According to the equivalent circuit method [7], there is a transformer coupling between the coil and the rest parts of the forming tool. Thus, an equivalent circuit (Figure 8) can simulate the operation of the forming tool. The equivalent circuit consists of resistances and inductances connected in series and in parallel, which represent every detail of the forming tool. The current is considered AC. This assumption is valid only for the first half period of the current pulse, during which the effect of the damping factor on the amplitude is small and, moreover, this is the most important period of time for the electro-magnetic forming process. Undoubtedly, this is an approximate method, but the obtained results are found to be close to experimental measurements [7].

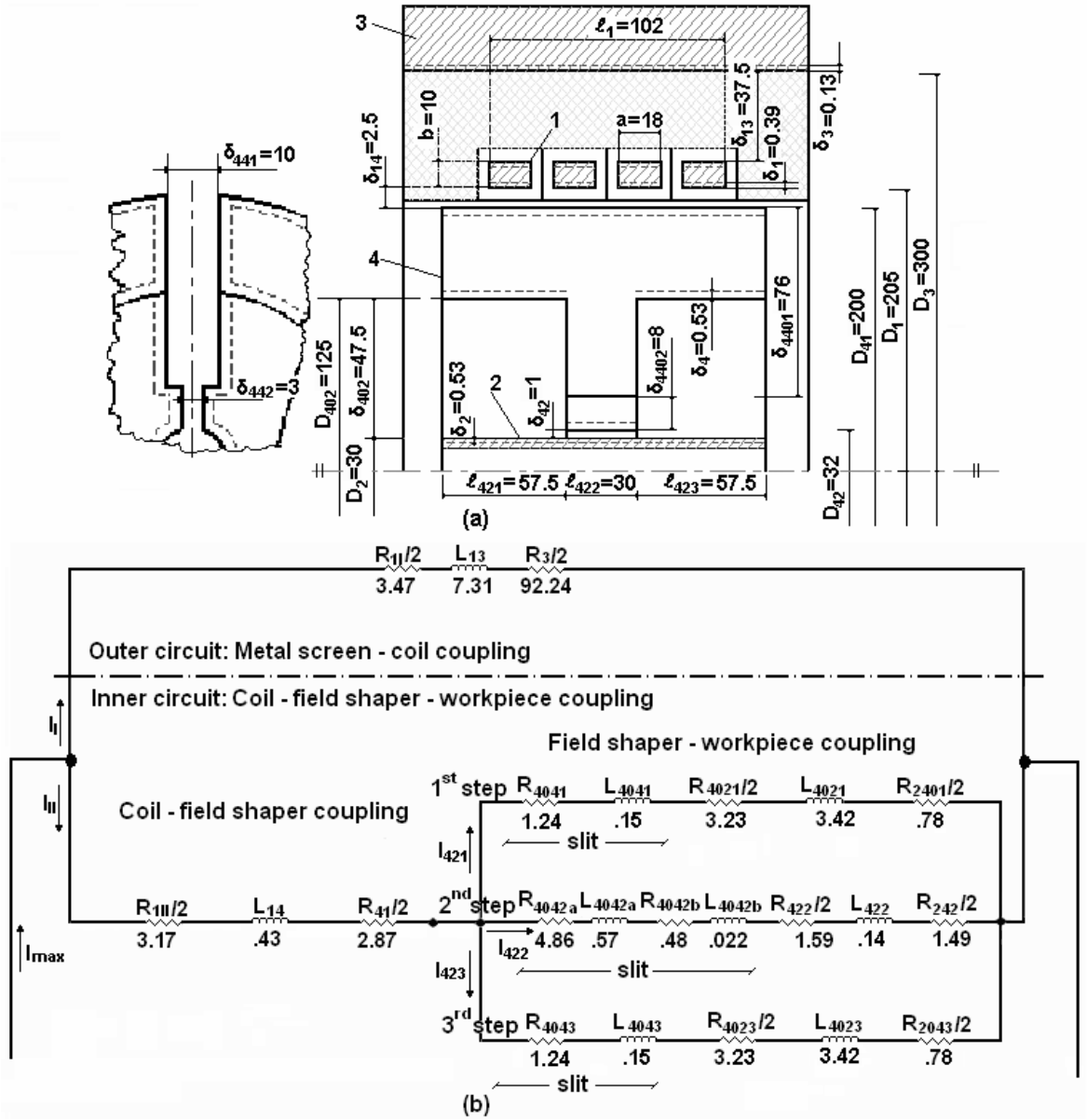

Figure 8: *(a) The equivalent scheme of the modelled forming tool and the relevant dimensions in mm and (b) The corresponding equivalent circuit with the relevant resistances and inductances in mΩ and μH respectively*

Taking into account that the inductances L_{14} and L_{422} correspond to the gap between the coil and the field shaper and between the middle step of the field shaper and the workpiece respectively, and applying the current and the voltage Kirchhoff's Laws in the equivalent circuit, then the currents I_{II} and I_{422} can be determined. So, the magnetic energy in the gaps between the coil and the field shaper and between the field shaper and the workpiece can be expressed by the following equations respectively:

$$E_{m14} = \frac{1}{2} \cdot L_{14} \cdot |I_{II}|^2 = \left(\frac{B_{14}^2}{2 \cdot \mu_o} \right) \cdot v_{14} \tag{6}$$

and

$$E_{m422} = \frac{1}{2} \cdot L_{422} \cdot \left| I_{422} \right|^2 = \left(\frac{B_{422}^2}{2 \cdot \mu_o} \right) \cdot v_{422} \tag{7}$$

where, v_{14} and v_{422} the volume of the corresponding gaps, given by the equations:

$$v_{14} = \left[1 - \frac{\delta_{441}}{\pi \cdot D_{41}} \right] \cdot \\ \cdot \left\{ 0.5 \cdot \pi \cdot \left[\left(D_1 + 2 \cdot \delta_1 \right) + \left(D_{41} - 2 \cdot \delta_4 \right) \right] \cdot \left(\delta_1 + \delta_4 + \delta_{14} \right) \cdot \left[\ell_1 + 0.5 \cdot \left(\delta_1 + \delta_4 + \delta_{14} \right) \right] \right\} \tag{8}$$

and

$$v_{422} = \left[1 - \frac{\delta_{442}}{\pi \cdot D_2} \right] \cdot \left\{ 0.5 \cdot \pi \cdot \left[\left(D_{42} + 2 \cdot \delta_4 \right) + \left(D_2 - 2 \cdot \delta_2 \right) \right] \cdot \left(\delta_4 + \delta_2 + \delta_{42} \right) \cdot \ell_{422} \right\} \tag{9}$$

excluding the slit region and taking into account the effective dimensions of the contributing conductors. Finally, the magnetic flux densities yield from Equations (6) and (7) and the corresponding calculated values are $B_{14} = B_{C\text{-}FS} = 4.6$ T and $B_{422} = B_{FS\text{-}W} = 11.3$ T respectively.